OUTDOOR PV PERFORMANCE EVALUATION OF THREE DIFFERENT MODELS: SINGLE-DIODE, SAPM AND LOSS FACTOR MODEL

Joshua S. Stein[1a], Juergen Sutterlueti[2], Steve Ransome[3], Clifford W. Hansen[1b], Bruce H. King[1c]
[1a] (Corresponding Author) Sandia National Laboratories, P.O. Box 5800 MS 1033, Albuquerque, NM 87185 USA. tel: (505)-845-0936, fax: (505)-844-2890, email: jsstein@sandia.gov
[1b] tel: (505) 284-1643, cwhanse@sandia.gov
[1c] tel: (505) 284-6571, bhking@sandia.gov
[2] TEL Solar, Haupstrasse 1a, 9477 Truebbach, juergen.sutterlueti@solar.tel.com
[3] SRCL, London, UK, +44 7515 565010; steve@steveransome.com; www.steveransome.com

ABSTRACT: This study examines the accuracy and value of three different PV module performance modeling approaches by calibrating selected performance models to outdoor IV data measured on different module technologies. We compare measured and modeled IV characteristics by examining the error distributions and correlations with time varying quantities to assess the accuracy of each model for the modules tested. The equivalent circuit diode models (e.g., PVsyst, PV*SOL, CEC, etc.) are popular, but include technology-specific corrections and calibration is challenging. Empirical models such as the Sandia PV Array Performance Model (SAPM) and TEL/SRCL "Loss Factors model" (LFM) are better able to represent technology performance differences and changes over time. Several of the SAPM coefficients lack of physical meaning whereas the LFM coefficients relate directly to IV characteristics. This study explores the strengths and weaknesses of each approach to model PV module and system performance with the goal of reducing prediction uncertainty and project risk, and improving the quality and value of PV system modeling and simulations.
Keywords: Modeling, Energy rating, Outdoor Testing, Characterization

1 INTRODUCTION

PV module performance models are used to estimate a module's IV characteristic as a function of irradiance and cell temperature, including spectral and reflection effects. A number of different model forms exist to fit measured IV curves. Some models represent the full IV curve (e.g., single diode equivalent circuit models such as PVsyst [1], PV*SOL [2], and the CEC model [3]) while others, such as the Sandia PV Array Performance Model (SAPM) [4] and the "TEL/SRCL" Loss Factors Model (LFM) [5-8], estimate only key points on the IV curve such as the maximum power point (*Vmp*, *Imp*), short circuit current (*Isc*), and open circuit voltage (*Voc*). The LFM also estimates performance losses due to series and shunt resistances.

This study quantitatively compares three PV module performance models in order to identify advantages and disadvantages of each approach in order to be able to predict performance. IV curves that were measured for a variety of PV module technologies while mounted on a two axis tracker in New Mexico are used for the comparison. These data are used to demonstrate differences between module models. Modules selected for this test include six commercially available modules (mono-Si, poly-Si, and CdTe) and six different CIGS modules from four manufacturers.

2 METHODS

Twelve test modules (Table 1) were used for all measurements in this paper. Each module was mounted on an Az/El 2-axis tracker (±0.5° accuracy) pointed at the sun for all measurements in this paper at Sandia National Laboratories (SNL) in Albuquerque, NM (~35.05° N, 106.54° W) and held normal to the sun. Preconditioning was performed according to manufacturer guidance. Each module was instrumented with three Type-T thermocouples along the module diagonal. The solar irradiance in the plane of the module was measured using a standard silicon reference cell PRC-Kochmann RS1, Berlin, DE). Global normal irradiance was measured using a standard pyranometer (Kipp& Zonen CM-21, Delft, NL) calibrated for off-angle performance. A co-located weather station provides redundant irradiance measurements.

Table I: Modules Compared in this Study

Number	Module	Number	Module
1	Mono-Si-1	7	CIGS-1
2	Mono-Si-2	8	CIGS-2
3	Mono-Si-3	9	CIGS-3
4	Poly-Si-1	10	CIGS-4
5	Poly-Si-2	11	CIGS-5
6	CdTe-1	12	CIGS-6

Note: CIGS modules are all preproduction modules

IV scans were performed on each module at 1-minute intervals over the entire day for several days to cover a range of clear and cloudy (diffuse) conditions. Each IV scan took approximately 5 seconds; between scans, each module was held at its maximum-power operating point. Irradiance before and after each trace was compared and used to filter out curves obtained during unstable irradiance conditions (e.g., irradiance changes >2%). Noise in the current near *Isc* would indicate variable irradiance during the trace. The average back surface temperature for each module was obtained from the three thermocouples.

Module temperature coefficients for *Isc*, *Voc*, *Imp* and *Vmp* were also measured outdoors for each module using test protocols developed at Sandia National Laboratories [9]. This measurement was performed near solar noon during stable, clear sky and calm wind conditions. An opaque cover was placed on the front surface of the module and it was allowed to cool to ambient temperature. The cover was then removed and the module exposed to sunlight and allowed to warm to equilibrium operating temperature. I-V scans were collected continuously as the module warmed to normal operating temperature.

Data for each module was collected over the course of several years. Thus, none of the data presented in this paper was collected simultaneously. Further, module performance was typically measured at different times of the year (e.g. one module might have been measured for a week in December, another module for a week in June).

In order to explore strengths and weaknesses of the different modeling approaches, we used these IV data to estimate parameters for each model (SAPM, LFM, and the CEC model) using methods that are described later. Next using the estimated parameters and measured environmental conditions we ran each model to predict the maximum power point (MPP) for each of the measured IV curves used for model calibration and compared the predictions with measurements. Distributions of error in predicted *Pmp*, *Imp*, and *Vmp* are compared between the models. We limited the focus of this study to the comparison between the IV models specifically and neglected an examination of the various methods used to correct for spectral effects, angle of incidence losses, etc. We did this by using "effective irradiance" (*Ee*) in place of measured irradiance as input to the performance models and by comparing data taken only while the module was normal to the sun on the tracker. The *Ee* quantity is discussed in next section.

2.1 Loss Factors Model

The Loss Factors Model (LFM) [5-8] was developed to fit measured outdoor IV curves to not only predict energy yield over time but also to detect and analyze the root causes of observed degradation and seasonal variation with physical meaning. It has been used by TEL to examine several years continuous data in Switzerland and Arizona studying degradation and seasonal annealing. For Sandia, it has been studied with data for a week or so to characterise each module. The model is based on a set of normalized parameters that describe each IV curve and a set of fitting coefficients that describe how these parameters vary with irradiance G_i and module temperature T_{module}. Given a measured IV curve (prefix = "m") and a reference IV curve at STC (prefix = "*r*"), the following six normalized LFM variables (prefix = "*n*") are defined [6,7]. *mVr* and *mIr* are coordinates of the intersection point of lines tangent to the ends of the measured IV curve as shown in the example in Fig 1.

1. $nIscT = \frac{mIsc}{rIsc} / G_i \times T_{CORR.Isc}$
2. $nRsc = \frac{mIr}{mIsc}$
3. $nImp = \frac{mImp}{mIr} \times \frac{rIsc}{rImp}$
4. $nVmp = \frac{mVmp}{mVr} \times \frac{rVoc}{rVmp}$
5. $nRoc = \frac{mVr}{mVoc}$
6. $nVocT = \frac{mVoc}{rVoc} \times T_{CORR.Voc}$

where $T_{CORR,Voc} = 1 + \beta_{Vmp} \times (25 - T_{module})$, $T_{CORR,Isc} = 1 + \alpha_{Imp} \times (25 - T_{module})$, and G_i is plane-of-array (POA) irradiance in suns. In the original versions of LFM, temperature coefficients for *Voc* and *Isc*, respectively, were used for the temperature corrections. We discovered in this study that the model performance is improved by using temperature coefficients associated with *Vmp* and *Imp*, respectively – an updated and more accurate version of the LFM will be published taking into consideration these findings for short term data.

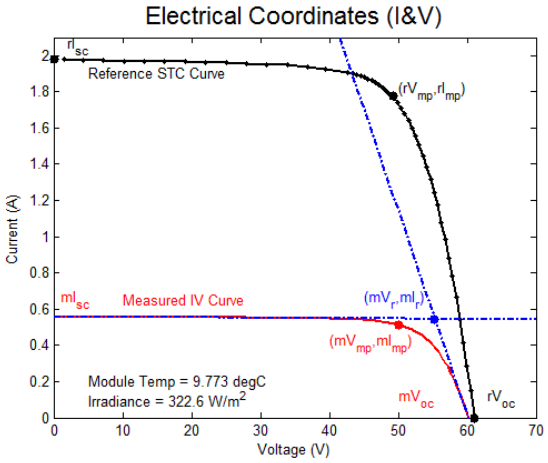

Figure 1. Example measured and reference IV curves showing key points in the electrical coordinate system (V, I).

A predictive model is developed by fitting each of these normalized parameters to G_i using the following functional form for each fit:

$$nf(G_i) = c_1 + c_2 \times ln(G_i) - c_3 \times {G_i}^2 .$$

As this is a normalised equation the values of c_1 will usually be 100±<10%, c_2 and c_3 will usually be 0±<10%. MPP can be then predicted (prefix = "*p*") at any irradiance and temperature conditions by first calculating the normalized LFM variables from the fitted equations and then evaluating the two equations below:

$$pImp = nIscT \times MMF \times nRsc \times nImp \times rImp \times G_i \div T_{CORR.Isc}$$

$$pVmp = nVmp \times nRoc \times nVocT \times rVmp \div T_{CORR.Voc}.$$

MMF is the spectral mismatch factor which can be calculated from measured spectrum and quantum efficiency of the PV cell (e.g., IEC 60904-7). In the previously published versions of the LFM model [6,7], *nIscT* is spectrally corrected using measured outdoor spectra. In our test setup in New Mexico we did not then have access to spectral data nor to the quantum efficiency of the test modules, both of which are needed to evaluate spectral mismatch. Instead we substituted "effective" irradiance (*Ee*) for the quantity $MMF \times G_i$ in the equation for *pImp*. *Ee* is determined from *mIsc*, *rIsc*, module temperature, and α_{Isc} (temperature coefficient for *Isc*) as (eq. 22 in [4]):

$$Ee = mIsc/[rIsc \times \{1 + \alpha_{Isc}(T_{module} - 25)\}].$$

This approach allows easier comparison between models and removes the additional uncertainties associated with irradiance and spectral mismatch. Because we are using α_{Imp} to temperature-correct *nImpT* and $\alpha_{Isc}$to calculate *Ee*, *nIscT* will not be equal to one, unless $\alpha_{Imp} = \alpha_{Isc}$.

Figure 2 displays an example of the normalized measurements corresponding to each variable in the LFM model, and the fitted functions of irradiance for each variable as specified above.

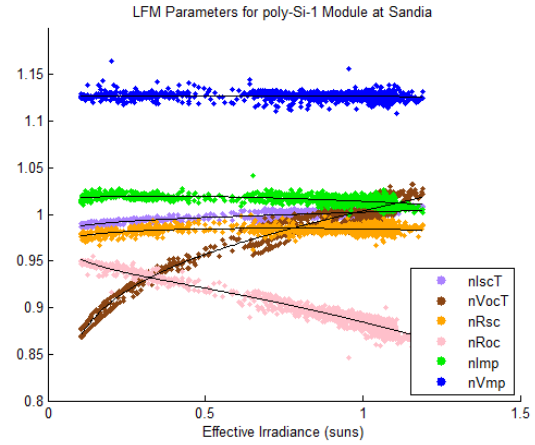

Figure. 2. LFM parameters as a function of irradiance with curve fits for the Poly-Si-1 module.

2.2 Sandia Array Performance Model (SAPM)

SAPM is an empirical model of module output at open-circuit, short-circuit and maximum power conditions. The fundamental equations in SAPM are described in detail in [4]. Coefficients for this model are obtained by fitting model equations to IV curves measured outdoors on a two-axis tracker [9].

2.3 California Energy Commission (CEC) Model

The CEC model is based on the conceptual "single diode" equivalent circuit shown in Figure 3 for a PV cell.

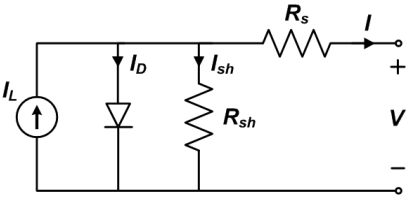

Fig. 3. Single diode equivalent circuit used to represent a PV cell.

Assuming identical cells obtains an equation for the IV curve of a PV module comprising N_s cells in series:

$$I_M = I_L - I_0\left[\exp\left(\frac{V_M + I_M N_s R_s}{n N_s V_T}\right) - 1\right] - \frac{V_M + I_M N_s R_s}{N_s R_{sh}}$$

where I_M and V_M are the current and voltage, respectively, of the module. The five parameters are primary to all single diode equivalent circuit models:

- I_L : light current (A)
- I_0 : diode reverse saturation current (A)
- R_s : series resistance (Ohm)
- R_{sh} : shunt resistance (Ohm)
- n : diode ideality factor (unitless)

Additional equations describe how these five parameters vary with irradiance and temperature; these equations vary among the various models (e.g., PVsyst [1], PV*SOL, and CEC [10]) which use the single diode equation. For our comparison we examined the CEC model which uses the following additional equations:

$$I_L = I_L\left(E, T_C\right) = \frac{E}{E_0}\left[I_{L0} + \alpha_{Isc}\left(T_C - T_0\right)\right]$$

$$I_O = I_{O0}\left[\frac{T_C}{T_0}\right]^3 \exp\left[\frac{1}{k}\left(\frac{E_g\left(T_0\right)}{T_0} - \frac{E_g\left(T_C\right)}{T_C}\right)\right]$$

$$E_g\left(T\right) = E_{g0}\left(1 - 0.0002677\left(T_C - T_0\right)\right)$$

$$R_{sh} = R_{sh}\left(E\right) = R_{sh0}\left(E_0/E\right)$$

where the subscript $\sim_0$ indicates a value at STC conditions. In the CEC model [10] both R_s and n are constant.

Single diode models are difficult to calibrate to data [11]. Most commonly, a single IV curve at STC conditions is used to determine the necessary parameter values [e.g., 12]. This approach implicitly assumes the additional equations correctly describe how parameters change with irradiance and temperature. Recently, Sandia National Laboratories has developed calibration methods that fit all equations for a single diode model to a set of measured IV curves [13] which permits evaluation of each equation's ability to describe a module's behavior. We used these techniques in our analysis.

2.4 Test Modules

Twelve modules were compared in this study. Their cell technologies and ID number are listed in Table 1.

2.5 Temperature Coefficients

To determine temperature coefficients for this study, we used IV curves measured during the outdoor thermal test, where the module was insulated from the back and exposed to full sun after being initially covered. During the test, the module heats rapidly until it reaches thermal equilibrium when the test ends. Measured *Voc* and *Vmp* were corrected for small variations in irradiance by typical methods. For example, for *Voc*:

$$Voc_{cor} = mVoc - \frac{N_s\, kn}{q}\ln\left(G_i\right)$$

where N_s is the number of cell in series, k is Boltzmann's constant (1.38066×10^{23} J/K), n is a representative diode ideality factor for each technology, and q is the elementary charge (1.60218×10^{-19} coulomb). Similar corrections are made for *Vmp*. Results are not very sensitive to the value of n; e.g., we assumed 1.1 to be representative for all silicon-based technologies. Figure 4 show an example of the analysis that determines temperature coefficients. Table II in the appendix lists the temperature coefficients for each module.

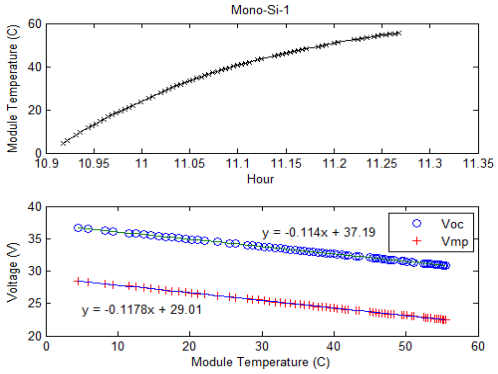

Figure 4: Example data and result from the thermal test to determine voltage temperature coefficients.

3 MODEL COMPARISON

Each model was run in a forward manner to predict performance for the measured conditions corresponding to each IV curve recorded during the electrical performance test. The models were evaluated by comparing predicted *Pmp*, *Imp*, and *Vmp* against measured values.

For the CEC model, the parameter estimation method [13] did not converge sufficiently to produce a reasonable predictive model for CIGS-4; therefore we do not show CEC model results for this module.

Figure 5 compares relative mean bias errors and relative root mean square errors between models for each module. The LFM model has the lowest bias errors, although the bias errors are quite low for all models (note 10^{-3} factor at top of y-axis). Except for module 6 (CdTe-1) and module 9 (CIGS-3), the relative RMSEs are quite similar between models.

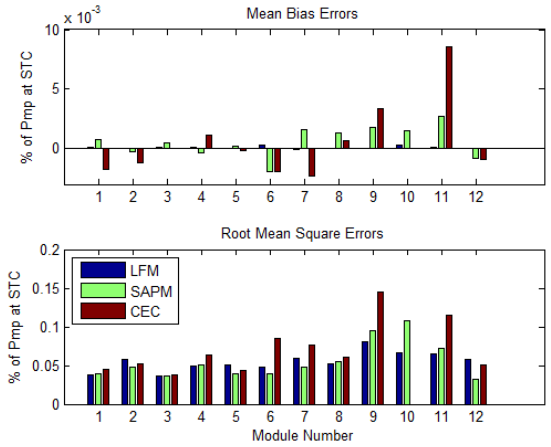

Figure 5: Mean bias and root mean square errors for *Pmp*. Modules numbers are listed in Table 1.

3.1 Residuals

Examination of model residuals of *Pmp*, *Imp*, and *Vmp* more closely show clear differences in how the three models perform with the test modules. Figures 6-8 show cumulative distributions of the residuals for each of the modules.

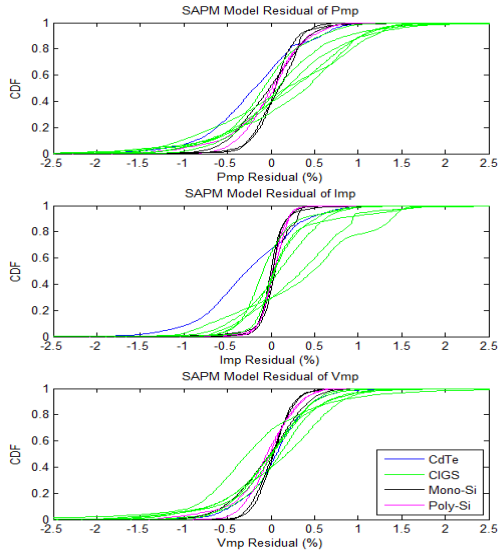

Figure 6: Cumulative distribution functions for residuals in *Pmp*, *Imp*, and *Vmp* for the SAPM model.

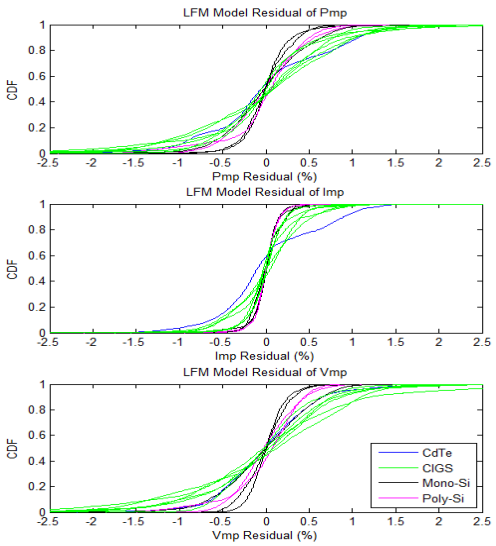

Figure 7: Cumulative distribution functions for residuals in *Pmax*, *Imax*, and *Vmax* for the LFM model.

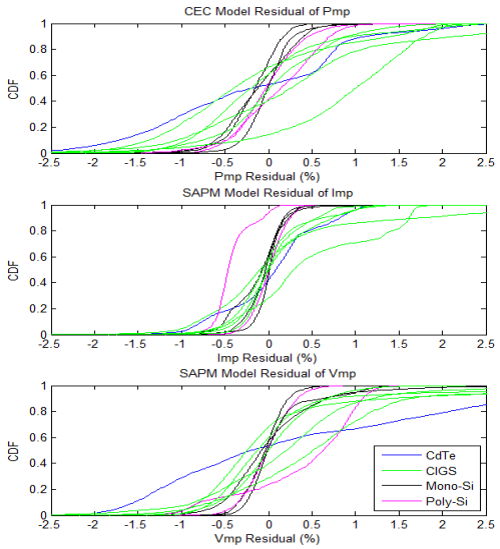

Figure 8: Cumulative distribution functions for residuals in *Pmax*, *Imax*, and *Vmax* for the CEC model.

4. DISCUSSION

The comparison between models illustrates that for most modules all three models can be calibrated to predict MPP with similar levels of accuracy. It is interesting to note that when predictions are examined in detail, certain models have distinct errors for one or more modules. For example the CdTe-1 module (blue line in Figures 6-8) show different error patterns for different models. The SAPM model slightly underestimated *Imp* for this module, resulting in a slight underestimate of *Pmp*. The underestimate of *Imp* results from SAPM's expression of *Imp* as quadratic in effective irradiance (i.e., with slightly negative but constant curvature), whereas the data show negative curvature that changes over the range of effective irradiance. In contrast, the LFM model exhibits a slight overestimate bias in Imp during certain conditions. For the CEC model, the CdTe-1 module stands out for not being well represented by the

model (largest variance in model residuals). For the CEC model, the relatively large prediction errors result from considering the series resistance as constant, whereas the values of series resistance estimated for each IV curve vary strongly with effective irradiance. The differences in performance between models based on the same IV data raise important concerns about criteria used to choose performance models. How does one ensure that the chosen model is valid for a selected module? Which model is most appropriate to use?

Once an accurate performance model is calibrated, it is valuable to be able to examine a module's model coefficients and say something about the health or condition of the module under test. One of the biggest drawbacks of the SAPM model is that the values of many of the individual model coefficients have little physical meaning and cannot be readily compared between modules. This is due to the use equations whose coefficients represent fitting parameters for functions with variables that are in engineering units (e.g., volts, amps, etc.) whose ranges can vary widely between different PV modules (e.g. c-Si modules typically have high *Isc* and low *Voc* values whereas thin film modules tend to have low *Isc* and high *Voc*). For the CEC model, although fitting parameters have physical units, the relationship between these parameters and module performance (e.g., between *Rsh* and *Vmp*) is mathematically complex and difficult to visualize. In contrast, the LFM model is based on fits to normalized variables in equations for points on the IV curve, thus the fitting parameters for different modules can easily be compared and used to discern important differences between modules.

Figure 2 shows a great example of the LFM variables vs. irradiance for a crystalline silicon module that is performing well (Poly-Si-1). *nVocT* increases with irradiance due to the logarithmic rise in *Voc* with temperature. *nRoc* decreases due to the series resistance loss increasing with the square of irradiance (e.g., loss ~ $I^2 \times Rseries$). Some scatter is present but the data trends are clear and consistent.

In contrast, the CdTe-1 module is an example where model fitting exposes a minor performance issue. Figure 9 shows the 6 LFM variables plotted against *Ee*. This plot displays an interesting feature, "synchronised" distinct traces above the *nVmp* fit and below the *nRoc* fit.

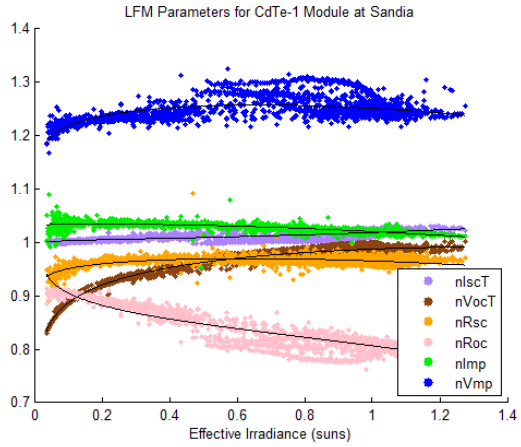

Figure 9: LFM variables vs. Ee for CdTe-1.

These traces (*nVmp*>1.27) occur during clear days when the wind speed increased and lowered module temperature to below 40C. Figure 10 demonstrates this as scatter plot of *nVmp* vs. T_{module} at high and low irradiance, which indicates clear and cloudy conditions, respectively as these measurements are made on a tracker.

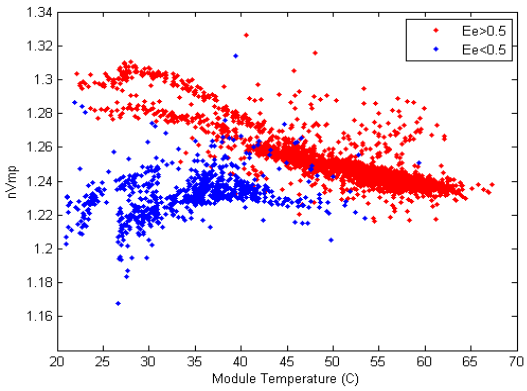

Figure 10: *nVmp* vs. T_{module} for CdTe-1.

We suspect that this behavior may indicate some level of metastability or defect in the module and may reflect a slight reversible Schottky rollover effect [e.g., 14, 15], possibly caused by the rapid temperature fluctuations.

CIGS-4, which is a preproduction prototype module, provides an example of a module with more serious performance issues. The LFM variables are plotted in Fig. 13 against *Ee*. In contrast with "optimal behaviour" from Fig 2, the low values of *nRoc* and *nRsc* at low irradiance indicates a poor performing module with highly nonlinear performance as a function of irradiance as if shunt resistance were decreasing with irradiance. Increasing *nVmp* with *Ee* relative to *nImp* provides clues to the source of the problem. The LFM plot clearly displays these relationships and provides valuable understanding that is not immediately evident from a set of SAPM or CEC module coefficients.

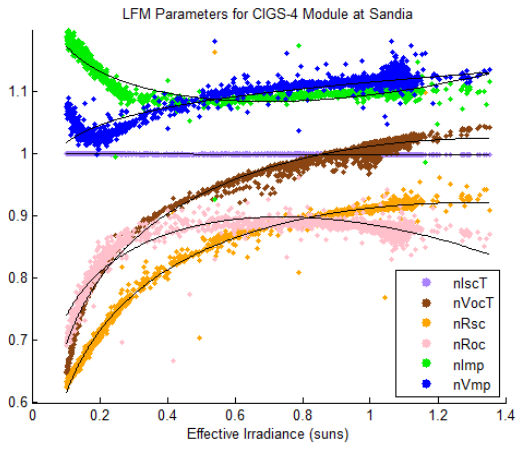

Figure 13: LFM variables vs. *Ee* for CIGS-4.

Plotting model residuals vs. time or other quantities can yield additional insights. For example, an examination of the model residuals vs. time (bottom plot in Fig. 11) for the CdTe-1 module indicates that module performance is improving during the period of measurement, likely due to well-known light soaking effects for CdTe. This observation indicates that the preconditioning routine may not have been sufficient to stabilize the module before testing. Similar indications of

metastable behavior were observed for CIGS-1, however in this case, the fill factor is seen to decrease over the time of the test.

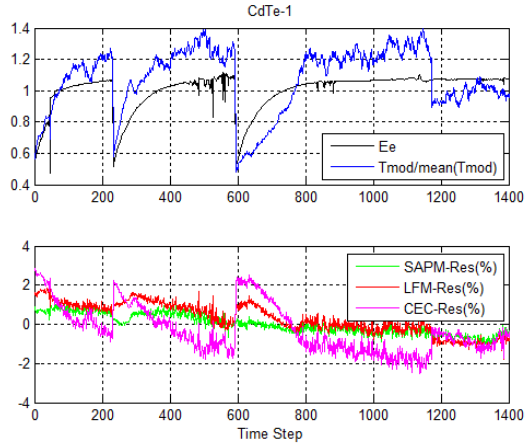

Figure 11: Top plot is of *Ee* and normalized T_{module} vs. time step. Bottom plot displays model residuals (% relative to *Pmp* at STC).

Plotting model residuals vs. independent variables (e.g., module temperature) can reveal model deficiencies. For example, model residuals for *Vmp* are plotted against module temperature in Figure 12. It is clear that the CEC model for this module results in a biased prediction of *Vmp* with errors correlated with temperature, which results in the larger variance for the CEC model for this module shown in Figure 8. This sensitivity of the CEC model residuals to temperature is evident for all of the thin film modules for which we were able to estimate parameters, but not for the c-Si and poly-Si modules, suggesting that some aspects of the CEC model itself may not be appropriate when applied to thin-film modules.

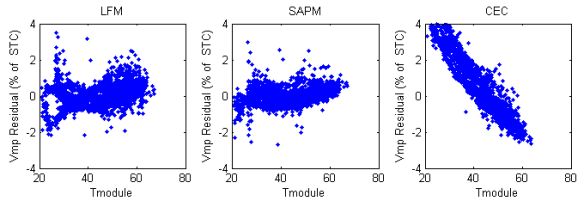

Figure 12: *Vmp* model residuals vs. T_{module}.

6. CONCLUSIONS

We have compared three different PV module models with fundamentally different formulations.

The CEC model displays the largest errors for certain modules and is difficult to fit (converge) for others. The CEC model is currently the only one of the three models able to predict the continuous IV curve, which may prove to be of increased importance in the future as system DC/AC ratios increase and PV systems are operated off their MPP (also possible with LFM and SAPM with small adaptations). However, the CEC model also appears to exhibit a strong sensitivity to temperature for the thin film modules for which we were able to derive coefficients. This suggests that there are still an opportunities for improving methods for estimation of model coefficients for single diode type models, especially for thin film modules. Developing methods to estimate these parameters remains an active research area.

The SAPM model resulted in similar bias errors to the CEC model and random errors comparable to the LFM model. The SAPM model coefficients do not provide diagnostic information about the relative "health" condition of the modules, since their parameters have no physical meaning.

The LFM model showed the lowest bias errors and comparable random errors to the SAPM. The data from Sandia resulted from a 2D tracker and needed small adaptions to get the same accurate curve fits as the TEL data on a fixed tilt.

We used temperature coefficients for *Imp* and *Vmp* rather than *Isc* and *Voc*. In addition, we substituted effective irradiance for measured irradiance to remove uncertainties related to spectral mismatch.

The LFM model has been shown to be able to fit a wide variety of modules of varying quality, but its unique strength is that it allows quick identification of strange performance patterns and provides insightful information on why performance is nonstandard. The LFM curve fit parameters have physical meaning since they relate directly to the behavior of the key points on the normalized IV curve with changing irradiance. By plotting the 6 normalized LFM variables with irradiance module health can be quickly assessed. An examination of these fits over time has been shown to be a valuable tool for detecting changes in performance over time (or season) [6].

The limitations of this work include: the use of only IV data collected on 2-axis tracker (no angle of incidence effects) and lack of field measured spectrum. Future work will include analyses using fixed tilt module IV data and also take advantage of new outdoor spectrometer capability at Sandia's test site. We also plan to focus on accurately representing performance of series and parallel connected arrays taking into account module variability and associated mismatch. IV curves from series connected strings of modules are currently being collected for this work. This step will assist the extension of module-scale modeling to modeling of an entire PV power plant.

Based on the results of this study, Sandia National Laboratories plans to add the LFM analysis methodology to its standard set of methods used for outdoor module characterization.

7. ACKNOWLEGEMENTS

Sandia is a multiprogram laboratory operated by Sandia Corporation, a Lockheed Martin Company, for the United States Department of Energy's National Nuclear Security Administration under contract DE-AC04-94AL85000.

8. REFERENCES

[1] A. Mermoud and T. Lejeune (2010). "Performance Assessment Of A Simulation Model For Pv Modules Of Any Available Technology," 25th

European Photovoltaic Solar Energy Conference, Valencia, Spain, 2010.
[2] PVSol, Valentin Software (2013). http://valentin-software.com/products/photovoltaics
[3] CEC (2013). "California Solar Initiative Incentive Calculators" from http://www.csi-epbb.com/documentation.aspx.
[4] King et al. (2004). "Photovoltaic Array Performance Model," Albuquerque, NM, Sandia National Laboratories.
[5] Sutterlueti, J., S. Ransome, et al. (2011). "Characterizing PV modules under outdoor conditions: What's most important for Energy Yield," EU PVSEC, Hamburg, Germany.
[6] Sellner, S., J. Sutterlueti, et al. (2012). Understanding Module Performance further: validation of the novel loss factors model and its extension to ac arrays. EU PVSEC. Frankfurt, Germany.
[7] Ransome, S., J. Sutterlueti, et al. (2012). "PV technology differences and discrepancies in modelling between simulation programs and measurements." 2012 38th IEEE Photovoltaic Specialists Conference (PVSC): 3061-3066.
[8] Sellner, S., J. Sutterlueti, et al. (2012). "Advanced PV module performance characterization and validation using the novel Loss Factors Model." 2012 38th IEEE Photovoltaic Specialists Conference (PVSC): 2938-2943.
[9] Hansen, C., et al. (2011). Parameter Uncertainty in the Sandia Array Performance Model for Flat-Plate Crystalline Silicon Modules. 37th IEEE Photovoltaics Specialists Conference, Seattle, WA.
[10] De Soto, W., et al. (2006). "Improvement and validation of a model for photovoltaic array performance." Solar Energy 80(1): 78-88.
[11] Hansen, C. W. (2013). Estimation of Parameters for Single Diode Models Using Measured IV Curves. 39th IEEE Photovoltaic Specialists Conference. Tampa, FL.
[12] A. P. Dobos. (2012). An Improved Coefficient Calculator for the California Energy Commission 6 Parameter Photovoltaic Module Model. *Journal of Solar Energy Engineering*, v. 134, 2012.
[13] Hansen, C.W. and Stein, J.S. (2013). Sensitivity of Single Diode Models for Photovoltaic Modules to Method Used for Parameter Estimation. 28th European Photovoltaic Solar Energy Conference, Paris, France.
[14] Bätzner, D. L., et al. (2000). Effect of Back Contact Metallization on the Stability of CdTe/CdS Solar Cells. 16th European Photovoltaic Solar Energy Conference, Glasgow, UK.
[15] Corwine, C. R., et al. (2004). "Copper inclusion and migration from back contact in CdTe solar cells." Solar Energy Materials and Solar Cells 82: 481-489.

Appendix A:

Table II: Temperature Coefficients for Test Modules.

Module Number	*aIsc* (%/°C)	*aImp* (%/°C)	*BVoc* (%/°C)	*BVmp* (%/°C)
1	0.03%	-0.03%	-0.29%	-0.37%
2	0.04%	-0.04%	-0.31%	-0.40%
3	0.05%	0.01%	-0.26%	-0.32%
4	0.07%	0.02%	-0.35%	-0.46%
5	0.06%	0.00%	-0.31%	-0.43%
6	0.03%	-0.04%	-0.27%	-0.24%
7	0.01%	-0.06%	-0.32%	-0.39%
8	0.00%	-0.04%	-0.33%	-0.39%
9	-0.01%	-0.07%	-0.33%	-0.41%
10	0.00%	0.00%	-0.33%	-0.41%
11	0.03%	-0.08%	-0.43%	-0.54%
12	-0.01%	-0.16%	-0.38%	-0.49%